

# Properties of entangled photon pairs generated in periodically poled nonlinear crystals

Jiří Svozilík and Jan Peřina Jr.

*Joint Laboratory of Optics of Palacký University and Institute  
of Physics of Academy of Sciences of the Czech Republic,  
17. listopadu 50A, 772 07 Olomouc, Czech Republic*

## Abstract

Using a rigorous quantum model a comprehensive study of physical properties of entangled photon pairs generated in spontaneous parametric down-conversion in chirped periodically-poled crystals is presented. Spectral, temporal, as well as spatial characteristics of photon pairs are analyzed. Spectral bandwidths, photon-pair flux, and entanglement area can be effectively controlled by chirping. Quantification of entanglement between photons in a pair is given. Splitting of entanglement area in the transverse plane accompanied by spectral splitting has been revealed. Using the model temperature dependencies of the experimental intensity profiles reported in literature have been explained.

## I. INTRODUCTION

The beginning of nonlinear quantum optics can be dated back to the sixties of the 20th century, when the first nonlinear optical phenomena were observed [1] owing to the discovery of the laser. The next milestone was reached twenty years later by Hong, Ou and Mandel who observed strong quantum correlations between photons in a photon pair generated in the process of spontaneous parametric frequency down-conversion [2]. These photon pairs represent the elementary quantum objects that can be correlated in time, space, momentum, energy, polarization or even orbital angular momentum. They have been used in many applications including tests of Bell's inequalities [3], quantum cryptography [4], quantum teleportation [5, 6], and metrology [7].

Many different structures emitting entangled photon pairs have been developed. Nonlinear bulk crystals [8] and nonlinear wave-guides belong to standard sources of these photon pairs nowadays. Also new sources based on photonic-crystal fibers [9, 10], layered photonic structures [11, 12, 13, 14], nonlinear cavities [15], and photonic nanostructures like quantum dots have been investigated.

However, periodically-poled crystals are distinguished from other photon-pair sources for two reasons [16, 17, 18]. High photon-pair fluxes are reached because of the use of materials with high nonlinearities due to quasi-phase-matching. On the other hand, chirping allows to generate photon pairs with extremely wide spectral bandwidths and subsequently extremely sharp temporal features. Such photon pairs are useful in many experiments, e.g., in quantum optical coherence tomography [19] or determination of tunnelling times [20]. Wide spectral bandwidths of entangled photon pairs make them prospective for parallel processing of quantum information.

In theory, description of chirped periodically-poled crystals has been restricted to simple more-less analytically soluble models up to now [16, 17, 18]. Properties of photon pairs in the transverse plane have not been addressed in these models. In the paper, we investigate spectral, temporal as well as spatial properties of the emitted photon pairs in detail using a complete theory. Special attention has been devoted to the role of chirping

parameter that is found extraordinarily useful in tailoring properties of photon pairs. Splitting of entanglement area that is accompanied by spectral splitting is predicted in this model. Also temperature dependencies of intensity profiles experimentally observed in [18] have been addressed using the model.

The model of spontaneous parametric down-conversion is introduced in Sec. II. Quantities characterizing photon pairs are defined in Sec. III. Spectral and temporal properties as well as entanglement of photons in a pair are discussed in Sec. IV. Properties of photon pairs in the transverse plane including entanglement area and temperature dependencies are analyzed in Sec. V. Conclusions are drawn in Sec. VI.

## II. MODEL OF SPONTANEOUS PARAMETRIC DOWN-CONVERSION

We use multi-mode description of spontaneous parametric down-conversion [21]. Each field, i.e. pump, signal and idler, is represented by plane-waves with given polarizations. Nonlinear process is described by first-order perturbation solution of Schrödinger's equation in the interaction picture. Interaction Hamiltonian  $\hat{H}_{\text{int}}$  is in the form:

$$\begin{aligned} \hat{H}_{\text{int}}(t) = & S4\pi^2\epsilon_0 \int_{-L}^0 dz \chi^{(2)}(z) : \mathbf{E}_p^{(+)}(z, t) \\ & \times \hat{\mathbf{E}}_s^{(-)}(z, t) \hat{\mathbf{E}}_i^{(-)}(z, t) + \text{H.c.} \end{aligned} \quad (1)$$

Symbol  $S$  denotes transverse area of the pump beam,  $\epsilon_0$  is permittivity of vacuum, and  $\chi^{(2)}(z)$  represents a third-order tensor of second-order nonlinear susceptibility that is assumed wavelength-independent. Symbol  $:$  is a shorthand for tensor  $\chi^{(2)}$  with respect to its three indices and H.c. replaces a Hermitian conjugated term. Symbol  $L$  denotes length of the nonlinear crystal. The strong pump field is described classically whereas the weak signal and idler fields are treated quantumly using operator amplitudes. An efficient nonlinear interaction is observed provided that  $x$ ,  $y$ , and  $z$  components of the wave vectors fulfil at least approximately phase matching conditions in the corresponding directions. Assuming

plane-wave pumping and sufficiently wide crystal perfect phase matching in the transverse plane (spanned by  $x$  and  $y$  variables) occurs.

Positive frequency part of pump-field amplitude  $\mathbf{E}_p^{(+)}$  has the form:

$$\mathbf{E}_p^{(+)}(z, t) = \sum_{\gamma=TM, TE} \int_{-\infty}^{\infty} d\omega_p \tilde{\mathbf{E}}_{p,\gamma}^{(+)}(z, \omega_p) \times \exp[i([\mathbf{k}_{p,\gamma}]_z z - \omega_p t)]. \quad (2)$$

The abbreviation TM (TE) stands for transversal magnetic (electric) waves,  $\omega_p$  is pump-field angular frequency,  $\mathbf{k}_{p,\gamma}$  the corresponding wave-vector, and  $\tilde{\mathbf{E}}_{p,\gamma}^{(+)}(z, \omega_p)$  spectrum of the positive-frequency part of the pump-field amplitude. Strong coherent pumping is assumed and so the depletion of the pump field can be neglected.

The signal and idler fields are described by negative-frequency parts of electric-field amplitude operators  $\hat{\mathbf{E}}_s^{(-)}$  and  $\hat{\mathbf{E}}_i^{(-)}$ , respectively, that can be written as follows [22]:

$$\hat{\mathbf{E}}_j^{(-)}(z, t) = \sum_{\xi=TM, TE} \int_{-\infty}^{\infty} d\omega_j \sqrt{\frac{\hbar\omega_j}{4\pi\epsilon_0 c n_\xi(\omega_j) S_\perp}} \mathbf{e}_{j,\xi}(\omega_j) \times \hat{a}_{j,\xi}^\dagger(\omega_j) \exp[-i([\mathbf{k}_{j,\xi}]_z z - \omega_j t)], \quad (3)$$

$j = s, i$ . Symbol  $\mathbf{e}_{j,\xi}(\omega_j)$  stands for polarization vector of a mode with frequency  $\omega_j$  and polarization  $\xi$  whereas  $\hat{a}_{j,\xi}^\dagger(\omega_j)$  represents the creation operator of this mode. Symbol  $\hbar$  denotes reduced Planck's constant,  $n_\xi(\omega_j)$  is the index of refraction and  $c$  is speed of light.

First-order solution of Schrödinger's equation gives the wave-function of an entangled two-photon state in the output plane of the crystal:

$$|\psi^{(2)}\rangle = -\frac{i}{\hbar} \int_{-\infty}^{\infty} dt \hat{H}_{\text{int}}(t) |\psi_{00}\rangle, \quad (4)$$

where  $|\psi_{00}\rangle$  denotes the initial signal- and idler-field vacuum state. Contributions described by higher orders of the perturbation solution are assumed to be small due to relatively low pumping intensity. Taking into account Eqs. (1), (2), (3), and (4) the wave function  $|\psi^{(2)}\rangle$  can be obtained in the form:

$$|\psi^{(2)}\rangle = \sum_{\alpha,\beta=TM, TE} \int_{-\infty}^{\infty} d\omega_s \int_{-\infty}^{\infty} d\omega_i \times \tilde{\mathcal{A}}_{\alpha\beta}(\omega_s, \omega_i) \hat{a}_{s,\alpha}^\dagger(\omega_s) \hat{a}_{i,\beta}^\dagger(\omega_i) |\psi_{00}\rangle. \quad (5)$$

Here,  $\tilde{\mathcal{A}}_{\alpha\beta}(\omega_s, \omega_i)$  denotes a two-photon spectral amplitude giving probability amplitude of emitting a signal photon at frequency  $\omega_s$  and polarization  $\alpha$  together with an idler photon at frequency  $\omega_i$  and polarization  $\beta$ . Two-photon amplitude  $\tilde{\mathcal{A}}_{\alpha\beta}$  can be expressed as [23, 24, 25]

:

$$\begin{aligned} \tilde{\mathcal{A}}_{\alpha\beta}(\omega_s, \omega_i) &= C_{\alpha,\beta}^\psi(\omega_s, \omega_i) \sum_{\gamma=TM, TE} \int_{-\infty}^{\infty} d\omega_p \int_{-L}^0 dz \\ &\times \int_{-\infty}^{\infty} dk_n \tilde{\chi}^{(2)}(k_n) : \mathbf{e}_{s,\alpha}(\omega_s) \mathbf{e}_{i,\beta}(\omega_i) \\ &\times \exp[i([\mathbf{k}_{p,\gamma}]_z - [\mathbf{k}_{s,\alpha}]_z - [\mathbf{k}_{i,\beta}]_z - k_n) z] \\ &\times \tilde{\mathbf{E}}_{p,\gamma}^{(+)}(0, \omega_p) \delta(\omega_p - \omega_s - \omega_i) \end{aligned} \quad (6)$$

where  $\tilde{\chi}^{(2)}$  is Fourier transform of function  $\chi^{(2)}(z)$  and  $k_n$  denotes a grid vector of poling. Alternatively, the crystal length can be given indirectly by number  $N_L$  of layers. Normalization function  $C_{\alpha,\beta}^\psi(\omega_s, \omega_i)$  has the form:

$$C_{\alpha,\beta}^\psi(\omega_s, \omega_i) = \frac{\pi\sqrt{\omega_s\omega_i}}{ic\sqrt{n_\alpha(\omega_s)n_\beta(\omega_i)}}. \quad (7)$$

Variations of second-order nonlinear susceptibility  $\chi^{(2)}$  along the  $z$ -axis can be described using the formula:

$$\chi^{(2)}(z) = \chi_0^{(2)} \text{sign}[\cos(k_{n0}z - \zeta z^2)] \text{rect}\left[\frac{z}{-L}\right]. \quad (8)$$

Symbol  $k_{n0}$  denotes a basic grid vector of poling and  $k_{n0} = \pi/l_0$  where  $l_0$  represents the length of the basic layer. Parameter  $\zeta$  characterizes chirping of the poled structure. Function  $\text{rect}(x)$  equals 1 for  $0 \geq x \geq 1$  and is zero otherwise. We note that periodical poling can be reached by applying strong static electric fields to domains (defined by contacts prepared by lithography) that invert the sign of nonlinear susceptibility  $\chi^{(2)}$  [17]. An other method is based on mapping an optical-field interference pattern to  $\chi^{(2)}$  nonlinearity that can be done provided that a nonlinear material is placed into a strong uv radiation [26].

### A. Simplified description using uniform poling

Formation of the spectral shape by interference from all layers can be studied analytically for uniform poling and cw pumping provided that we restrict ourselves to a scalar modes and consider propagation along the  $z$  axis only. The two-photon amplitude  $\tilde{\mathcal{A}}$  can then be expressed as:

$$\begin{aligned} \tilde{\mathcal{A}}(\omega_s, \omega_i) &= C^\psi(\omega_s, \omega_i) \tilde{\mathbf{E}}_p^{(+)}(\omega_{p0}) \delta(\omega_{p0} - \omega_s - \omega_i) \\ &\times \int_{-L}^0 dz \chi^{(2)}(z) \exp[i\Delta k z]; \end{aligned} \quad (9)$$

$\Delta k = k_p - k_s - k_i$ . Integration along the crystal in Eq. (9) can be replaced by the sum of contributions coming from each layer and then the two-photon amplitude  $\tilde{\mathcal{A}}$  takes

the form:

$$\begin{aligned} \tilde{\mathcal{A}}(\omega_s, \omega_i) &= C^\psi(\omega_s, \omega_i) \tilde{E}_p^{(+)}(\omega_{p0}) \delta(\omega_{p0} - \omega_s - \omega_i) \\ &\times l_o \text{sinc} \left[ \frac{\Delta k l_o}{2} \right] \frac{\sin [(\Delta k l_o - \pi) N_L / 2]}{\sin [(\Delta k l_o - \pi) / 2]} \\ &\times \exp \left[ -i(\Delta k l_o + \pi) \frac{N_L}{2} - i \frac{\pi}{2} \right]. \end{aligned} \quad (10)$$

Symbol  $l_o$  introduced in Eq. (10) denotes the length of one layer ( $l_o = L/N_L$ ). Function sinc in Eq. (10) originates in phase mismatch of one typical layer whereas superposition of down-converted fields from all layers gives the remaining part of the formula in Eq. (10) that resembles the well-known expression describing interference of a finite number of waves. Maximum value of the two-photon amplitude  $\tilde{\mathcal{A}}$  in Eq. (10) is reached if the sin function in the denominator is zero. This happens under the usual quasi-phase-matching condition  $\Delta k = \pi(n+1)/l_o$ ,  $n$  being an integer. The number of emitted photon-pairs at the corresponding frequencies is then proportional to  $N_L^2$ . The expression in Eq. (10) also indicates that the spectral width of the signal or idler field is proportional to  $1/N_L$  for cw pumping.

### III. CHARACTERISTICS OF PHOTON PAIRS EMITTED IN PERIODICALLY POLED CRYSTALS

Number of generated photon pairs  $N$  (per 1 s in cw regime) can be easily calculated from two-photon spectral amplitude  $\tilde{\mathcal{A}}$  given in Eq. (6):

$$N = \int_{-\infty}^{\infty} d\omega_s \int_{-\infty}^{\infty} d\omega_i |\tilde{\mathcal{A}}(\omega_s, \omega_i)|^2. \quad (11)$$

Energy spectrum  $S_{s,i}(\omega_{s,i})$  for the signal or idler field is determined similarly with the formula:

$$S_{s,i}(\omega_{s,i}) = \hbar \omega_{s,i} \int_{-\infty}^{\infty} d\omega_{i,s} |\tilde{\mathcal{A}}(\omega_s, \omega_i)|^2. \quad (12)$$

Schmidt's decomposition of the two-photon spectral amplitude  $\tilde{\mathcal{A}}$  into the dual basis can be used to quantify entanglement between signal and idler photons. Two-photon spectral amplitude  $\tilde{\mathcal{A}}(\omega_s, \omega_i)$  can then be expressed as

$$\tilde{\mathcal{A}}(\omega_s, \omega_i) = \sum_{n=1}^{\infty} \lambda_n \psi_n(\omega_s) \phi_n(\omega_i), \quad (13)$$

where  $\lambda_n$  are eigenvalues corresponding to base functions  $\psi_n$  and  $\phi_n$ . The base functions  $\psi_n$  and  $\phi_n$  are determined as solutions of the integral equations:

$$\int K_s(\omega, \acute{\omega}) \psi_n(\acute{\omega}) d\acute{\omega} = \lambda_n^2 \psi_n(\omega), \quad (14)$$

$$\int K_i(\omega, \acute{\omega}) \phi_n(\acute{\omega}) d\acute{\omega} = \lambda_n^2 \phi_n(\omega). \quad (15)$$

Entropy of entanglement  $E$  [27] defined as:

$$E = - \sum_{n=1}^{\infty} \lambda_n^2 \log_2 \lambda_n^2 \quad (16)$$

is used for quantification of entanglement. The higher the entropy  $E$ , the stronger the entanglement. The number of effective independent modes useful in Schmidt's decomposition is given by cooperation parameter  $K$  [28]:

$$K = \frac{1}{\sum_{n=1}^{\infty} \lambda_n^4}. \quad (17)$$

Temporal properties of photons in a pair can only be measured indirectly using interferometers. Relative time delay between photons in a pair can be determined in Hong-Ou-Mandel interferometer [29]. Normalized coincidence-count rate  $R_n(\tau)$  in this interferometer is expressed in the form:

$$R_n(\tau) = 1 - \rho(\tau) \quad (18)$$

and

$$\begin{aligned} \rho(\tau) &= \frac{1}{R_0} \int_{-\infty}^{\infty} dt_a \int_{-\infty}^{\infty} dt_b \\ &\times \text{Re} [\mathcal{A}(t_a, t_b - \tau) \mathcal{A}^*(t_b, t_a - \tau)] \\ &= \frac{1}{(2\pi)^2 R_0} \int_{-\infty}^{\infty} d\omega_s \int_{-\infty}^{\infty} d\omega_i \\ &\times \text{Re} [\tilde{\mathcal{A}}(\omega_s, \omega_i) \tilde{\mathcal{A}}^*(\omega_i, \omega_s) \exp(i\tau [\omega_i - \omega_s])]; \end{aligned} \quad (19)$$

Re denotes the real part of an argument. Symbol  $R_0$  is a normalization constant;  $R_0 = \lim_{\tau \rightarrow \infty} \rho(\tau)$ .

### IV. TEMPORAL AND SPECTRAL PROPERTIES OF PHOTON PAIRS, ENTANGLEMENT

The analysis is done for a periodically-poled nonlinear uniaxial crystal LiNbO<sub>3</sub>. Having in mind optical-fiber applications we consider cw plain-wave pumping at central wavelength  $\lambda_{p0} = 752.5$  nm. The signal and idler fields have wavelengths  $\lambda_{s0} = \lambda_{i0} = 1505$  nm ( $\lambda_{s0} = 1392.1$  nm and  $\lambda_{i0} = 1637.8$  nm) in the spectrally-degenerate (spectrally-non-degenerate) case. Assuming uniform poling the length identical for all layers is determined such that quasi-phase matching is reached for TM polarizations of all interacting fields at given central frequencies assuming collinear propagation. Since the studied material is anisotropic and we consider the optical axis parallel to the  $y$  axis, polarizations of all interacting fields correspond to extra-ordinary waves in collinear geometry. The length of layers for the spectrally-degenerate (spectrally-non-degenerate) case equals 8.9000  $\mu\text{m}$  (8.9286  $\mu\text{m}$ ).

If chirping in poling is assumed, the length of layer in the middle of the structure equals that for uniform

poling. The value of used chirping parameter  $\zeta$  ( $\zeta = 1 \times 10^{-6} \mu\text{m}^{-2}$ ) corresponds to the case in which shorter layers occur at the beginning of the crystal whereas longer layers are at the end of the crystal. We note that if the value of chirping parameter  $\zeta$  is sufficiently small, layer lengths depend more-less linearly on their positions. We also note that the effect of multiple reflections at crystal boundaries that leads to fast spectral oscillations (typical for a Fabry-Perot etalon [30]) occurs in periodically-poled crystals. However, we suppress them in our analysis by making local averaging of the signal- and idler-field spectra. This is in accord with usual experimental conditions in which these oscillations are smoothed out by a final spectral resolution of detectors.

Note that, the Fourier transform of Eq. (8) contains several spectral components. The component  $+k_n$  assures phase-matching at the central frequencies mentioned above. However, the component with  $-k_n$  also exists but cannot provide phase matching in the considered frequency range for the studied nonlinear crystal and so we omit it in further investigations.

### A. Spectrum and number of generated photon pairs

Typical spectra for both frequency-degenerate and frequency-non-degenerate down-conversion for uniform as well as chirped poling are shown in Fig. 1.

Fast modulation in these spectra has its origin in interference of two-photon amplitudes coming from different nonlinear layers of the crystal as expressions in Eqs. (10) and (12) indicate. In frequency-non-degenerate case and for uniform poling, there occur two peaks centered at different frequencies (see Fig. 1b). These contributions mutually interfere in the frequency region where they overlap. Chirped poling leads to wide broadening of the signal- and idler-field spectra, as demonstrated in Fig. 1a,b. The reason is that two-photon amplitudes from different layers have shifted ranges of the emitted signal- and idler-field frequencies and so when two-photon amplitudes from all layers are superposed, a much broader range of frequencies is covered. However this broadening is at the expense of lowering photon-pair emission rates. This occurs because nonlinear layers of different lengths and generating different two-photon amplitudes do not admit perfect constructive interference at optimum frequencies (as it occurs for uniform chirping). We also note that wider spatial emission angles occur for the higher values of chirping and so a considerable portion of the emitted signal does not contribute to the studied collinear case.

Successive forming of the signal-field spectrum as the number  $N_L$  of layers increases is depicted in Fig. 1c for uniform poling. Already two layers (that form the basic element of the structure) provide a spectrum that prefers the area around the central frequency. As the curves in

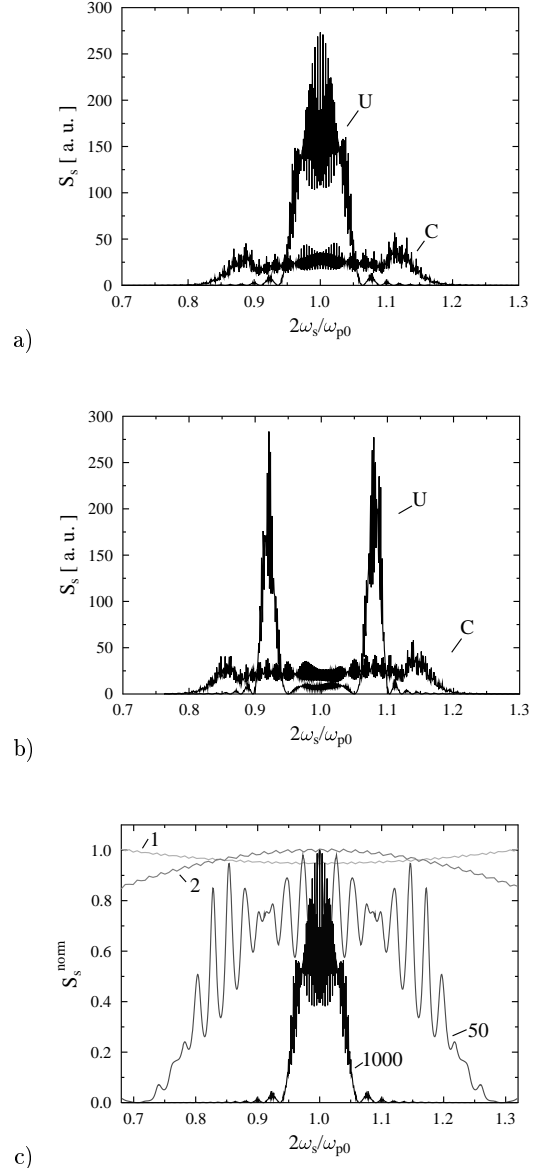


FIG. 1: Energy spectrum  $S_s$  for a) spectrally degenerate and b) spectrally non-degenerate down-conversion. Curves denoted as U (C) are appropriate for uniform (chirped) poling of the crystal;  $N_L = 1000$  in a) and b). Forming of normalized energy spectrum  $S_s^{\text{norm}}$  with the increasing number  $N_L$  of layers is documented in c) for uniform poling, spectral degeneration, and  $N_L = 1, 2, 50$ , and 1000.

Fig. 1c document the larger the number  $N_L$  of layers the narrower the spectrum [compare the expression in Eq. (10)].

Number  $N$  of generated photon pairs and signal- and idler-field spectral widths are the most important parameters of a photon-pair source in many applications. We show their dependence on the number  $N_L$  of layers (giving length  $L$  of the crystal) and chirping parameter  $\zeta$  in

## B. Fourth-order interference of a photon pair

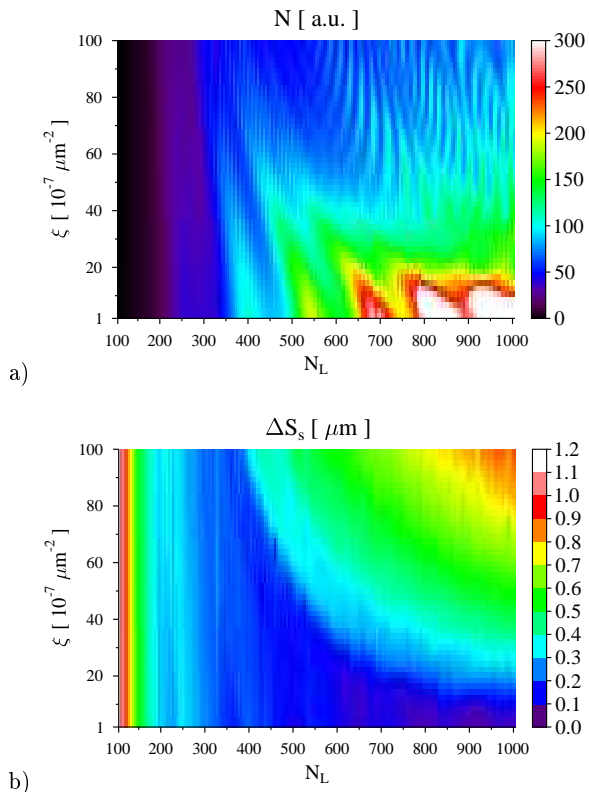


FIG. 2: (Color online) Contour plots of a) number  $N$  of generated photon pairs and b) spectral width  $\Delta S_s$  (FWHM) of the signal field as functions of the number of layers  $N_L$  and chirping parameter  $\zeta$ . Frequency degenerate case is assumed.

Fig. 2. We can observe the following general tendencies. Provided that  $\zeta$  is fixed increasing number  $N_L$  of layers gives higher numbers  $N$  of generated photon pairs but lowers spectral widths of the signal and idler fields. On the other hand and keeping  $N_L$  fixed increasing values of chirping parameter  $\zeta$  lead to decreasing of the number  $N$  of generated photon pairs and broader signal- and idler-field spectra.

Defined spectral widths of the signal and idler fields are required in many applications. The spectral widths are determined by the lengths of the first and last nonlinear layers in a crystal with chirped poling. Number  $N$  of generated photon pairs increases naturally with increasing number  $N_L$  of layers. Since lengths of the first and last layers are fixed, a larger number  $N_L$  of layers means a lower value of chirping parameter  $\zeta$ . Our numerical investigations have revealed that the product of number  $N$  of generated photon pairs and chirping parameter  $\zeta$  is roughly constant ( $N\zeta \approx \text{const}$ ) in this case. These observations allow to design easily structures with defined spectra and photon-pair emission rates.

Hong-Ou-Mandel interferometer giving fourth-order interference pattern allows to determine entanglement time from the profile of fourth-order interference pattern obtained by varying a mutual time delay between the signal and idler photons. Entanglement time gives a typical time window in which an idler photon is detected in this specific interferometer provided that its twin signal photon has already been detected. Entanglement time does not bear any information about the instant of a signal-photon detection. Entanglement time defined this way does depend on dispersion present in the paths of the signal and idler photons in general. However, if the same amount of dispersion is present in the signal-photon and idler-photon paths entanglement time is not affected [24]. In case of cw pumping, entanglement time is even not sensitive to even orders of material dispersion in the paths of two photons from a pair [31]. On the other hand, also sum-frequency generation can be used to define another typical time constant called correlation time (defined in optical-field coherence theory) [32]. Correlation time characterizes a true temporal shape of a biphoton (as given by the amplitude of a two-photon temporal amplitude) and is sensitive to dispersion. Careful dispersion compensation is experimentally required to observe the sharpest temporal features as possible.

If we consider frequency degenerate case, both photons in a pair are indistinguishable (are described by identical wave-functions) and we observe visibility 100% in a Hong-Ou-Mandel interferometer. Different central frequencies of the signal and idler fields lead to partial distinguishability of two photons and, as a consequence, the loss of visibility occurs (see Fig. 3a). Moreover, the signal and idler photons propagate at different group velocities and occur at the output of the crystal with nonzero relative mutual delay, that is determined from the shift of the dip position in the interference pattern. Also oscillations at the difference of the central signal- and idler-field frequencies occur. Low visibility is usually observed in this case because of complex interference of two-photon amplitudes coming from different layers. We note that the inclusion of third- and higher-odd-order dispersion terms has lead to small oscillations visible in Fig. 3a. Width of the coincidence-count interference pattern  $R_n(\tau)$  is mainly given by first-order dispersion properties of the crystal (for details see, e.g., [23])

Width  $\Delta\tau$  of the coincidence-count rate  $R_n$  increases with the increasing number  $N_L$  of layers concerning uniform poling (see Fig. 3b), in agreement with decreasing signal- and idler-field spectral widths. On the other hand, width  $\Delta\tau$  increases for smaller numbers  $N_L$  of layers whereas it decreases for larger numbers  $N_L$  of layers for chirped poling. This behavior can be related to the behavior of the signal- and idler-field spectral widths (see Fig. 2b): the wider the spectrum the smaller the width  $\Delta\tau$ . If number  $N_L$  of layers is sufficiently large, the width  $\Delta\tau$  decreases with increasing values of chirping param-

eter  $\zeta$  that makes spectral widths wider (see Fig. 3c). Several applications (e.g. quantum optical coherence tomography [19], determination of ultrashort temporal intervals [20]) require as short entanglement times as possible. Highly chirped crystals are then needed as sources of photon pairs giving the widest possible signal- and idler-field spectra.

### C. Entropy of entanglement

Entropy of entanglement  $E$  can be used to quantify the strength of mutual spectral entanglement between the signal and idler photons. Technically, integral equations in Eqs. (14) and (15) are discretized and converted this way into the problem of matrix diagonalization. Division has to be sufficiently close which is indicated by a large number of eigenvalues lying close to zero. Eigenvalues of Schmidt's decomposition do not depend on additional phase variations introduced by dispersion present in paths of the signal and idler photons. This can be deduced from the definition of kernels  $K_s$  and  $K_i$  [33] that are proportional to the reduced statistical operators of the signal and idler photons, respectively. These phase variations only affect phases of the complex base functions  $\psi_n$  and  $\phi_n$  occurring in the decomposition of two-photon spectral amplitude  $\tilde{A}$  in Eq. (13).

Entropy of entanglement  $E$  behaves similarly as signal- and idler-field spectral widths. The wider the spectra, the higher the entropy  $E$ . This means, that the higher the number  $N_L$  of layers in a uniformly poled crystal the lower the entropy  $E$ . Assuming chirped poling, entropy  $E$  decreases until a certain number  $N_{L0}$  of layers is reached and then increases (see Fig. 4). Cooperativity parameter  $K$  behaves similarly (see Fig. 4) as entropy  $E$ . We note that the wider the signal- and idler-field spectra the larger the number of eigenvalues  $\lambda_n$  needed in Schmidt's decomposition and as a consequence greater values of cooperativity parameter  $K$  and entropy  $E$  occur.

## V. SPATIAL PROPERTIES OF PHOTON PAIRS, CORRELATION AREA

### A. Intensity cross-section of the down-converted fields

A typical cross section of the signal-field photon number  $N_s$  for uniform poling is displayed in Fig. 5a where p-polarized signal and idler fields degenerate in frequency have been assumed. This means that the signal and idler photons propagate as extraordinary waves. The signal and idler fields propagate in general as a mixture of TE and TM waves at different emission angles, but the difference between TE and TM waves is small because of small values of radial emission angles and so the pattern of cross section is nearly spherically symmetric and occurs for radial emission angles  $\vartheta_s$  lower than 5 deg. The

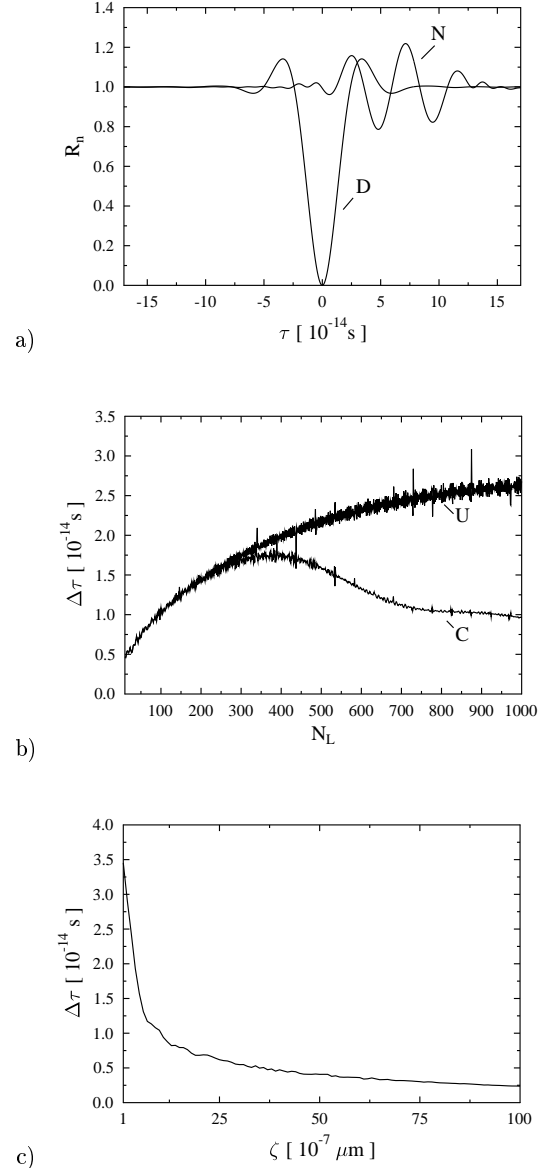


FIG. 3: a) Normalized coincidence-count rate  $R_n$  in Hong-Ou-Mandel interferometer as a function of relative time delay  $\tau$  for spectrally degenerate (D) and non-degenerate (N) down-conversion in a uniformly poled crystal. b) Width  $\Delta\tau$  (FWHM) of the interference dip in normalized coincidence-count rate  $R_n$  as a function of number  $N_L$  of layers for uniform (U) and chirped (C) poling. c) Width  $\Delta\tau$  as it depends on chirping parameter  $\zeta$ . Frequency degeneration is assumed;  $N_L = 1000$ ,  $\zeta = 1 \times 10^{-6} \mu\text{m}^{-2}$

highest numbers  $N$  of generated photon pairs are found in the vicinity of  $\vartheta_s = 0$  deg because the structure is optimized for collinear interaction.

Comparison of Figs. 5a and b reveals that chirping of poling practically does not change the emission angles. It mainly reduces the number  $N$  of generated photon

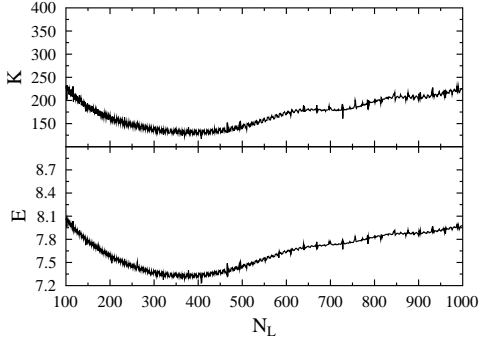


FIG. 4: Entropy  $E$  and cooperativity parameter  $K$  as they depend on number  $N_L$  of layers. Frequency degeneration as well as chirped poling are assumed;  $\zeta = 1 \times 10^{-6} \mu\text{m}^{-2}$ .

pairs in the middle of the emission pattern, i.e. at the emission angles at which the conditions for constructive interference of fields from different layers are worse in case of chirped poling. As a consequence, a relatively wide plateau replaces a typical peak found for uniform poling (see Fig. 5c for cuts of the cross-sections). We note that the idler twin of a signal photon is emitted into a direction given by phase-matching conditions both in the transverse plane and along the  $z$  axis.

Signal- and idler-field emission spectra are broad for all emission angles as Fig. 6 showing signal-field energy spectrum  $S_s$  documents. There occurs splitting of the signal-field energy spectrum  $S_s$  for radial emission angles  $\vartheta_s$  greater than 2 deg. The use of frequency filters thus allows to modify the emission-cone cross-section. For example, removal of the central part of the energy spectrum  $S_s$  leaves the emission-cone cross section in the form of a concentric ring.

## B. Correlation area of photon pairs

Correlation area determines possible emission directions of an idler photon [described by radial ( $\vartheta_i$ ) and azimuthal ( $\psi_i$ ) emission angles] which twin, i.e. signal photon, has been observed in a given direction defined by emission angles  $\vartheta_s$  and  $\psi_s$ . Because the crystal is not infinitely long and also the pump beam is not infinitely broad entanglement area has finite width that can be characterized by typical widths of the distribution giving probability of emission of an idler photon in a given direction. We denote them as  $\Delta\vartheta_i$  and  $\Delta\psi_i$  in the radial and azimuthal directions, respectively. Qualitatively, the longer the crystal the smaller the correlation area. Also the broader the transverse profile of the pump beam the smaller the correlation area.

There occurs splitting of correlation area into two parts in radial direction for emission angles that are farther from the optimum emission angle  $\vartheta_{s0}$  for which the struc-

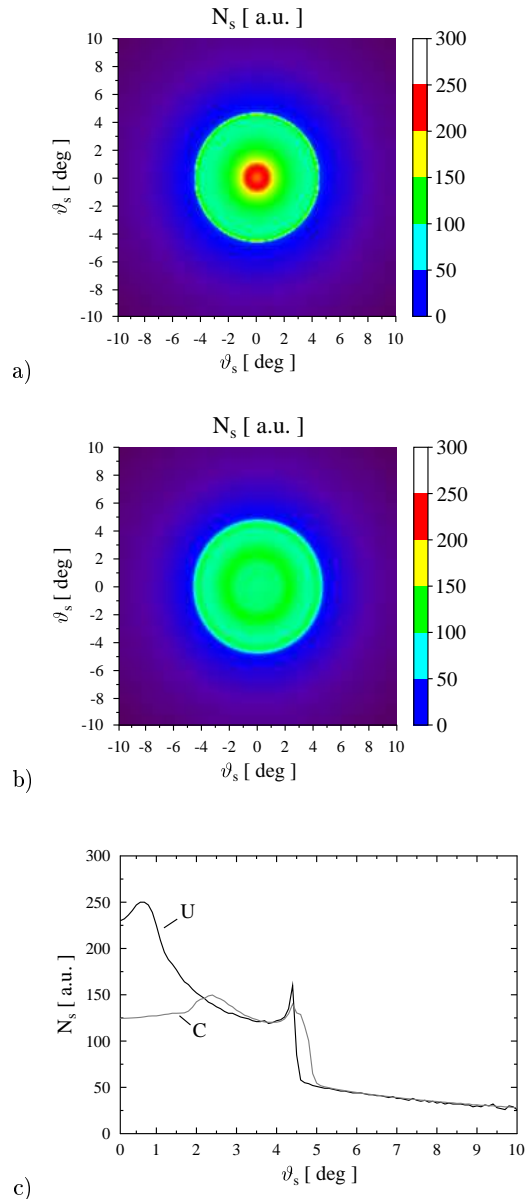


FIG. 5: (Color online) Contour plot of the cross-section of the signal-field photon number  $N_s$  projected onto hemisphere with radial emission angle  $\vartheta_s$  and azimuthal emission angle  $\psi_s$  (determines rotation angle around the center of the graph) for a) uniform and b) chirped poling. c) Cut of signal-field photon number  $N_s$  along the  $y$  axis ( $\psi_s = 0$  deg) traced by radial emission angle  $\vartheta_s$  for uniform (U) and chirped (C) poling. Frequency degeneration is assumed;  $\zeta = 1 \times 10^{-6} \mu\text{m}^{-2}$ ,  $N_L = 1000$ .

ture was designed. Considering uniform poling and structure optimized for collinear interaction, this splitting is clearly visible in Fig. 7a for radial emission angles  $\vartheta_s$  greater than 0.5 deg. Splitting in radial emission angle is accompanied by splitting in frequencies, i.e. frequency spectra of each part are separated (compare Figs. 7b and 6). Chirping of poling leads to blurring of correlation ar-

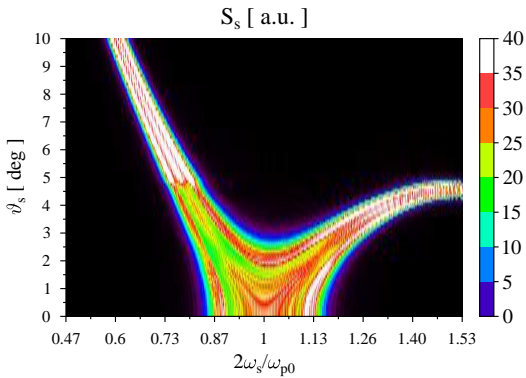


FIG. 6: (Color online) Contour plot of signal-field energy spectrum  $S_s$  as a function of signal-field emission angle  $\vartheta_s$  assuming chirped poling and degenerate spectrum;  $\zeta = 1 \times 10^{-6} \mu\text{m}^{-2}$ ,  $N_L = 1000$ .

reas, as documented in Fig. 7b. This is natural, because chirping provides broader spectra of the signal and idler fields that allow to fulfill phase-matching conditions in a wider area of emission angles. As is evident from Fig. 7b chirping partially conceals splitting of correlation area. Because width of correlation area is a monotonous function of chirping parameter  $\zeta$  (see Fig. 8), photon pairs with the required width of correlation area can be generated from poled crystals with appropriate chirping. We note that width of correlation area is an important parameter whenever wave-functions of two photons overlap.

### C. Temperature tuning of the intensity cross-section

Properties of the emitted photon pairs in the transverse plane can be controlled by temperature of the crystal as has been experimentally demonstrated in [18] for chirped periodically poled stoichiometric LiTaO<sub>3</sub>. The change of temperature causes changes in values of indices of refraction and also widths of layers undergo a certain temperature shift. As a consequence, temperature can be used to tune a sample into resonance where phase-matching conditions are perfectly fulfilled. If temperature changes from its optimum value, shift in emission directions is observed (see Fig. 9). If the crystal is optimized for collinear geometry, a spot occurring under optimum conditions is replaced by a concentric ring. The greater the declination of temperature from its optimum value the greater the diameter of this ring. If the crystal is highly chirped, this ring is smoothed and a disc is observed. Width of the spot as well as width of the ring depend strongly on bandwidth of frequency filters placed in front of detectors. The wider the bandwidth, the wider the spot and ring.

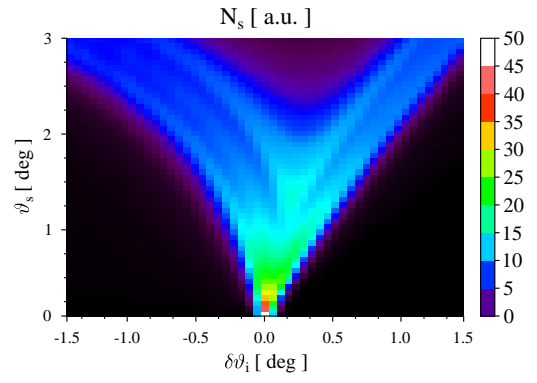
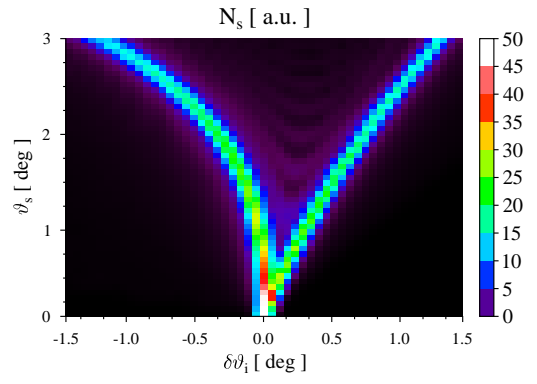


FIG. 7: (Color online) Contour plots showing the cut of correlation area along the idler-field radial emission angle  $\vartheta_i$  ( $\vartheta_i = \vartheta_i^{\text{opt}} + \delta\vartheta_i$ ,  $\vartheta_i^{\text{opt}}$  is given by optimum phase-matching conditions corresponding to a given  $\vartheta_s$ ) as it depends on signal-field radial emission angle  $\vartheta_s$ . Frequency-degenerate emission of p polarized signal and idler photons along the  $y$  axis is considered both for a) uniform and b) chirped poling;  $N_L = 1000$ ,  $\zeta = 1 \times 10^{-6} \mu\text{m}^{-2}$ .

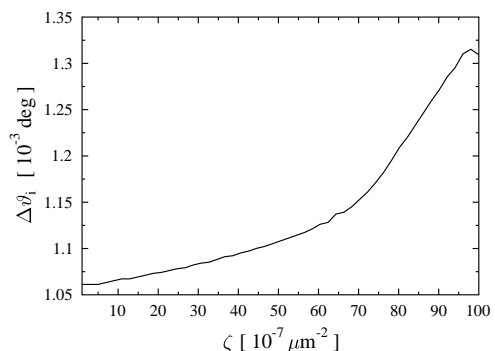


FIG. 8: Width  $\Delta\vartheta_i$  of correlation area in radial direction as a function of  $\zeta$  for collinear geometry and frequency non-degenerate case. The signal and idler photons are p polarized;  $N_L = 1000$ .



investigations of their rich physical properties.

### Acknowledgments

Support by projects IAA100100713 of GA AV ČR, COST 09026, MSM6198959213, and LC06007 of the Czech Ministry of Education is acknowledged. J.P. also thanks project 1M06002 of the Czech Ministry of Education.

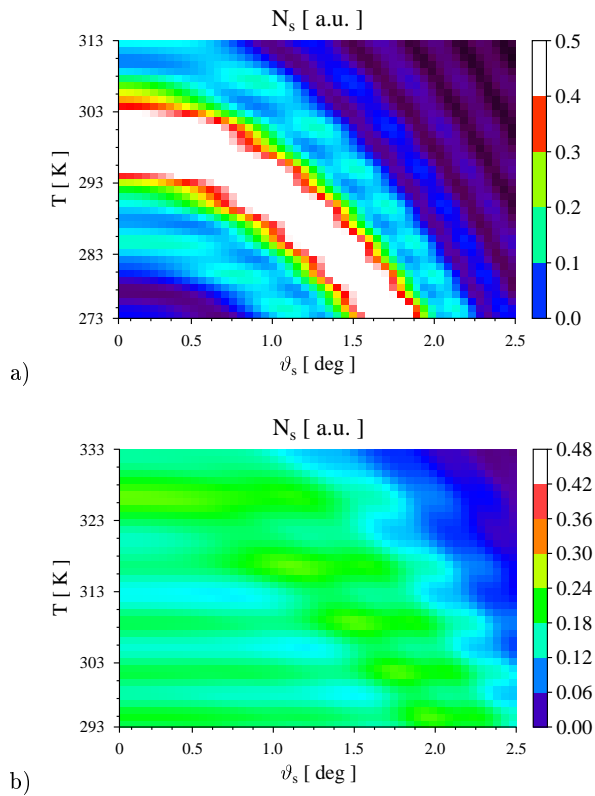


FIG. 9: (Color online) Contour plots giving the signal-field photon number  $N_s$  along the  $y$  axis parameterized by radial emission angle  $\vartheta_s$  as it depends on temperature  $T$ . The signal and idler photons are p polarized. Chirped poling with a)  $\zeta = 1 \times 10^{-7} \mu\text{m}^{-2}$  and b)  $\zeta = 1 \times 10^{-6} \mu\text{m}^{-2}$  is considered;  $N_L = 1000$ . Spectrally degenerate photons are filtered with narrow-band filter 14 THz wide.

## VI. CONCLUSIONS

A comprehensive study of physical properties of entangled photon pairs generated in chirped periodically-poled nonlinear crystals has been done using a rigorous model of spontaneous parametric down-conversion. Spectral, temporal, and spatial characteristics have been addressed. Ultra-wide spectra, high photon fluxes as well as entanglement areas can be conveniently controlled by chirping parameter. Ultra-wide spectra are responsible for high values of entanglement of photons in a pair that can be useful for quantum-information processing. The experimentally observed intensity profiles of the down-converted fields in the form of discs or rings with temperature-dependent parameters have been theoretically explained in this model. It has been revealed that complex interference of photon pairs from different layers leads to splitting of correlation area that is accompanied by spectral splitting. The presented results have shown that chirped periodically-poled crystals are not only promising as useful sources of photon pairs for many applications but they also remain interesting for

- 
- [1] P. A. Franken, A. E. Hill, C. W. Peters, and G. Weinreich, *Phys. Rev. Lett.* **7**, 118 (1961).
- [2] R. Ghosh, C. K. Hong, Z. Y. Ou, and L. Mandel, *Phys. Rev. A* **34**, 3962 (1986).
- [3] G. Weihs, T. Jennewein, C. Simon, H. Weinfurter, and A. Zeilinger, *Phys. Rev. Lett.* **81**, 5039 (1998).
- [4] C. H. Bennett, G. Brassard, and N. D. Mermin, *Phys. Rev. Lett.* **68**, 557 (1992).
- [5] D. Boschi, S. Branca, F. De Martini, L. Hardy, and S. Popescu, *Phys. Rev. Lett.* **80**, 1121 (1998).
- [6] D. Bouwmeester, J. Pan, K. Mattle, M. Eibl, H. Weinfurter, and A. Zeilinger, *Nature* **390**, 575 (1997).
- [7] A. Migdall, *Physics Today* **52** (1999).
- [8] M. H. Rubin, D. N. Klyshko, Y. H. Shih, and A. V. Sergienko, *Phys. Rev. A* **50**, 5122 (1994).
- [9] X. Li, P. L. Voss, J. E. Sharping, and P. Kumar, *Phys. Rev. Lett.* **94**, 053601 (2005).
- [10] J. Fulconis, O. Alibart, W. Wadsworth, P. Russell, and J. Rarity, *Opt. Express* **13**, 7572 (2005).
- [11] J. Peřina, Jr., M. Centini, C. Sabilia, M. Bertolotti, and M. Scalora, *Phys. Rev. A* **73**, 033823 (2006).
- [12] M. Centini, J. Peřina, Jr., L. Sciscione, C. Sabilia, M. Scalora, M. J. Bloemer, and M. Bertolotti, *Phys. Rev. A* **72**, 033806 (2005).
- [13] A. N. Vamivakas, B. E. A. Saleh, A. V. Sergienko, and M. C. Teich, *Phys. Rev. A* **70**, 043810 (2004).
- [14] J. Peřina, Jr., M. Centini, C. Sabilia, M. Bertolotti, and M. Scalora, *Phys. Rev. A* **75**, 013805 (2007).
- [15] J. Shapiro and N. Wong, *J. Opt. B: Quantum Semiclass. Opt.* **2**, L1 (2000).
- [16] S. E. Harris, *Phys. Rev. Lett.* **98**, 063602 (2007).
- [17] D. S. Hum and M. M. Fejer, *Comptes Rendus Physique* **8**, 180 (2007).
- [18] M. B. Nasr, S. Carrasco, B. E. A. Saleh, A. V. Sergienko, M. C. Teich, J. P. Torres, L. Torner, D. S. Hum, and M. M. Fejer, *Phys. Rev. Lett.* **100**, 183601 (2008).
- [19] S. Carrasco, J. P. Torres, L. Torner, A. Sergienko, B. E. A. Saleh, and M. C. Teich, *Opt. Lett.* **29**, 2429 (2004).
- [20] A. M. Steinberg, P. G. Kwiat, and R. Y. Chiao, *Phys. Rev. Lett.* **71**, 708 (1993).
- [21] L. Mandel and E. Wolf, *Optical Coherence and Quantum Optics* (Cambridge University Press, Cambridge, 1995).
- [22] W. Vogel and D.-G. Welsch, *Lectures on Quantum Optics* (Akademie Verlag, Berlin, 1994).
- [23] T. E. Keller and M. H. Rubin, *Phys. Rev. A* **56**, 1534 (1997).
- [24] J. Peřina, Jr., A. V. Sergienko, B. M. Jost, B. E. A. Saleh, and M. C. Teich, *Phys. Rev. A* **59**, 2359 (1999).
- [25] G. Di Giuseppe, L. Haiberger, F. De Martini, and A. V. Sergienko, *Phys. Rev. A* **56**, R21 (1997).
- [26] C. L. Sones, A. C. Muir, Y. J. Ying, S. Mailis, R. W. Eason, T. Jungk, A. Hoffmann, and E. Soergel, *Appl. Phys. Lett.* **92**, 072905 (2008).
- [27] C. K. Law, I. A. Walmsley, and J. H. Eberly, *Phys. Rev. Lett.* **84**, 5304 (2000).
- [28] C. K. Law and J. H. Eberly, *Phys. Rev. Lett.* **92**, 127903 (2004).
- [29] C. K. Hong, Z. Y. Ou, and L. Mandel, *Phys. Rev. Lett.* **59**, 2044 (1987).
- [30] B. Saleh and M. Teich, *Fundamentals of Photonics* (Wiley, New York, 1991).
- [31] A. M. Steinberg, P. G. Kwiat, and R. Y. Chiao, *Phys. Rev. A* **45** (1992).
- [32] S. E. Harris and S. Sensarn, in *Proceedings of the Ninth Rochester Conference on Coherence and Quantum Optics* (University of Rochester, 2007), pp. 65–71.
- [33] J. Peřina, Jr., *Phys. Rev. A* **77**, 013803 (2008).